Journal of the Korean Physical Society, Vol. 63, No. 1, July 2013, pp. 104∼113

Sparsely-synchronized Brain Rhythm in a Small-world Neural Network

Sang-Yoon Kim
Research Division, LABASIS Corporation, Chunchon 200-702, Korea

Woochang Lim*
Department of Science Education, Daegu National University of Education, Daegu 705-115, Korea

(Received 18 April 2013, in final form 28 May 2013)

Sparsely-synchronized cortical rhythms, associated with diverse cognitive functions, have been observed in electric recordings of brain activity. At the population level, cortical rhythms exhibit small-amplitude fast oscillations while at the cellular level, individual neurons show stochastic firings sparsely at a much lower rate than the population rate. We study the effect of network architecture on sparse synchronization in an inhibitory population of subthreshold Morris-Lecar neurons (which cannot fire spontaneously without noise). Previously, sparse synchronization was found to occur for cases of both global coupling (*i.e.*, regular all-to-all coupling) and random coupling. However, a real neural network is known to be non-regular and non-random. Here, we consider sparse Watts-Strogatz small-world networks which interpolate between a regular lattice and a random graph via rewiring. We start from a regular lattice with only short-range connections and then investigate the emergence of sparse synchronization by increasing the rewiring probability p for the short-range connections. For $p = 0$, the average synaptic path length between pairs of neurons becomes long; hence, only an unsynchronized population state exists because the global efficiency of information transfer is low. However, as p is increased, long-range connections begin to appear, and global effective communication between distant neurons may be available via shorter synaptic paths. Consequently, as p passes a threshold p_{th} ($\simeq 0.044$), sparsely-synchronized population rhythms emerge. However, with increasing p, longer axon wirings become expensive because of their material and energy costs. At an optimal value p^*_{DE} ($\simeq 0.24$) of the rewiring probability, the ratio of the synchrony degree to the wiring cost is found to become maximal. In this way, an optimal sparse synchronization is found to occur at a minimal wiring cost in an economic small-world network through trade-off between synchrony and wiring cost.

PACS numbers: 87.19.lm, 87.19.lc
Keywords: Sparsely-synchronized brain rhythm, Small-world network
DOI: 10.3938/jkps.63.104

I. INTRODUCTION

Recently, much attention has been paid to brain rhythms in health and disease [1, 2]. Particularly, we are interested in cortical rhythms, observed in awake behaving states, which are associated with diverse cognitive functions (*e.g.*, sensory perception, feature integration, selective attention, and memory formation) [3]. At the population level, local field potential recordings show synchronous small-amplitude fast oscillations [*e.g.*, beta rhythm (15 - 30 Hz), gamma rhythm (30 - 100 Hz), and sharp-wave ripple (100 - 200 Hz)], while spike trains of individual neurons are typically stochastic and sparse [4–6]. Thus, single-cell behavior differs markedly from the population behavior. These sparsely-synchronized rhythms are in contrast to the fully-synchronized large-amplitude slow rhythms observed in quiet sleep states [7,8]. Fully-synchronized oscillations may occur in a network of spiking suprathreshold neurons above a threshold in the absence of noise or for weak noise. As is well known, full synchronization may be well described in the framework of conventional models of coupled oscillators because individual neurons behave regularly as clocklike oscillators and fire at the population frequency [9]. However, such coupled-oscillator models are not adequate for describing sparse synchronization because individual neurons fire stochastically and intermittently as Geiger counters. Brunel *et al.* [10] developed a framework to describe sparse synchronization by taking an opposite view from that of coupled oscillators. Under the condition of strong external noise, suprathreshold spiking neurons (above a threshold) discharge stochastic firings as Geiger counters which form an asynchronous population state. This asynchronous state may be destabilized,

*E-mail: woochanglim@dnue.ac.kr

and synchronous oscillation emerges when inhibitory recurrent feedback becomes sufficiently strong. For this case, the average total (external excitatory plus recurrent inhibitory) input current into individual neurons is subthreshold, but irregular and intermittent firings are triggered when fluctuations (due to noise in the external and the recurrent inputs) cross a threshold. Thus, a sparsely-synchronized rhythm with stochastic and intermittent discharges appears. In addition to suprathreshold neurons, subthreshold neurons below the threshold (which cannot fire spontaneously without noise) also exist. These subthreshold neurons exhibit irregular and intermittent firings in the presence of moderate noise. Sparsely-synchronized rhythms are also found to emerge via cooperation of noise-induced spikings of subthreshold inhibitory neurons [11].

So far, sparse synchronization has been studied only in all-to-all networks where every neuron is coupled to every other neuron and in random networks [10,11]. In a local cortical circuit, synaptic connections are known to be sparse, and the connectivity has a complex topology (*e.g.*, small-worldness and scale-freeness) that is neither regular nor completely random [12–16]. Hence, many recent studies on diverse subjects of neurodynamics have been done in complex networks [17, 18] such as small-world networks with predominantly local connections and rare long-distance connections [19–31] and scale-free networks with a few percent of hub neurons with an exceptionally large number of connections [32–36]. Here, we study sparse synchronization in the Watts-Strogatz model for small-world networks which interpolates between short-range regular lattice and random network via rewiring [37]. A sparse regular lattice with only short-range connections has high clustering (*i.e.*, high cliquishness of a typical neighborhood), and hence local efficiency of information transfer becomes high [38]. However, due to long average synaptic path length (*i.e.*, typical separation between two neurons represented by average number of synapses between two neurons along the minimal path), global efficiency of information transfer becomes low [38], and hence occurrence of global synchronization becomes difficult. On the other hand, a sparse random network with poor clustering has a short average path length, and hence global communication between distant neurons becomes easily available. As in [37], we start from a local regular lattice, increase the rewiring probability p for the short-range connections, and then long-range short-cuts that connect distant neurons begin to appear. The average path length can be dramatically decreased only by a few short-cuts, while the clustering coefficient remains to be high. Thus, in a range of small p small-world networks with short path lengths and high clustering appear. Their topology is intermediate between regular lattice and random network.

This paper is organized as follows. In Sec. II, we describe the biological small-world network consisting of inhibitory subthreshold conductance-based Morris-Lecar neurons whose synaptic coupling is modeled in terms of synaptic kinetics controlled by GABAergic synaptic time constants. By increasing the rewiring probability p, we investigate emergence of sparsely synchronized rhythm in Sec. III. For the regular connection of $p = 0$, the global efficiency of information transfer is low due to long average path length, and hence an unsynchronized population state exists. However, with increasing p, long-range connections begin to appear, and global effective communication between distant neurons may be available via shorter synaptic paths. Consequently, the unsynchronized state is destabilized and then sparsely synchronized population rhythm emerges when p passes a threshold p_{th} ($\simeq 0.044$). However, as p is increased, the network axon wiring length becomes longer due to long-range connections. Longer axonal projections are expensive due to their material and energy costs. Hence, we must take into consideration the axon wiring economy for the dynamical efficiency because wire economy is an important constraint of the brain evolution [3,12,23,39–44]. At an optimal value p^*_{DE} ($\simeq 0.24$) of the rewiring probability, a dynamical efficiency factor given by the ratio of the synchrony degree to the axon wiring cost is found to become maximal. In this way, an optimal sparse synchronization is found to occur via compromise between synchrony and wiring cost at a minimal wiring cost in an economic small-world network. Finally, a summary is given in Section IV.

II. SMALL-WORLD NETWORK OF INHIBITORY SUBTHRESHOLD MORRIS-LECAR NEURONS

We consider a small-world network of N sparsely-coupled subthreshold neurons equidistantly placed on a one-dimensional ring of radius $N/2\pi$. Here, we employ a directed Watts-Strogatz model for small-world network which interpolates between short-range regular lattice and random network via rewiring [37]. As an element in our neural system, we choose the conductance-based Morris-Lecar (ML) neuron model with voltage-gated ion channels, originally proposed to describe the time-evolution pattern of the membrane potential for the giant muscle fibers of barnacles [45,46]. The population dynamics in this small-world neural network is governed by a set of the following differential equations:

$$C\frac{dv_i}{dt} = -I_{ion,i} + I_{DC} + D\xi_i - I_{syn,i}, \quad (1a)$$

$$\frac{dw_i}{dt} = \phi\frac{(w_\infty(v_i) - w_i)}{\tau_R(v_i)}, \quad (1b)$$

$$\frac{ds_i}{dt} = \alpha s_\infty(v_i)(1 - s_i) - \beta s_i, \quad i = 1, \cdots, N, \quad (1c)$$

where

$$I_{ion,i} = I_{Ca,i} + I_{K,i} + I_{L,i} \quad (2a)$$

$$= g_{Ca} m_\infty(v_i)(v_i - V_{Ca}) \quad (2b)$$
$$+ g_K w_i (v_i - V_K) + g_L (v_i - V_L), I_{syn,i}$$
$$= \frac{J}{d_i^{in}} \sum_{j(\neq i)}^{N} w_{ij} s_j(t)(v_i - V_{syn}), \quad (2c)$$
$$m_\infty(v) = 0.5\,[1 + \tanh\{(v - V_1)/V_2\}], \quad (2d)$$
$$w_\infty(v) = 0.5\,[1 + \tanh\{(v - V_3)/V_4\}], \quad (2e)$$
$$\tau_R(v) = 1/\cosh\{(v - V_3)/(2V_4)\}, \quad (2f)$$
$$s_\infty(v_i) = 1/[1 + e^{-(v_i - v^*)/\delta}]. \quad (2g)$$

Here, the state of the ith neuron at a time t (measured in units of ms) is characterized by three state variables: the membrane potential v_i (measured in units of mV), the slow recovery variable w_i representing the activation of the K^+ current (*i.e.*, the fraction of open K^+ channels), and the synaptic gate variable s_i denoting the fraction of open synaptic ion channels. In Eq. (1a), C represents the capacitance of the membrane of each neuron, and the time evolution of v_i is governed by four kinds of source currents.

The total ionic current $I_{ion,i}$ of the ith neuron consists of the calcium current $I_{Ca,i}$, the potassium current $I_{K,i}$, and the leakage current $I_{L,i}$. Each ionic current obeys Ohm's law. The constants g_{Ca}, g_K, and g_L are the maximum conductances for the ion and the leakage channels, and the constants V_{Ca}, V_K, and V_L are the reversal potentials at which each current is balanced by the ionic concentration difference across the membrane. Since the calcium current $I_{Ca,i}$ changes much faster than the potassium current $I_{K,i}$, the gate variable m_i for the Ca^{2+} channel is assumed to always take its saturation value $m_\infty(v_i)$. On the other hand, the activation variable w_i for the K^+ channel approaches its saturation value $w_\infty(v_i)$ with a relaxation time $\tau_R(v_i)/\phi$, where τ_R has a dimension of ms and ϕ is a (dimensionless) temperature-like time scale factor.

Each ML neuron is also stimulated by using the common DC current I_{DC} and an independent Gaussian white noise ξ_i [see the 2nd and the 3rd terms in Eq. (1a)] satisfying $\langle \xi_i(t) \rangle = 0$ and $\langle \xi_i(t)\, \xi_j(t') \rangle = \delta_{ij}\, \delta(t - t')$, where $\langle \cdots \rangle$ denotes the ensemble average. The noise ξ is a parametric one that randomly perturbs the strength of the applied current I_{DC}, and its intensity is controlled by using the parameter D.

The ML neuron may exhibit either type-I or type-II excitability, depending on the system parameters [46]. Throughout this paper, we consider the case of type-II excitability where $g_{Ca} = 4.4$ mS/cm^2, $g_K = 8$ mS/cm^2, $g_L = 2$ mS/cm^2, $V_{Ca} = 120$ mV, $V_K = -84$ mV, $V_L = -60$ mV, $C = 20$ μF/cm^2, $\phi = 0.04$, $V_1 = -1.2$ mV, $V_2 = 18$ mV, $V_3 = 2$ mV, and $V_4 = 30$ mV. As I_{DC} passes a threshold in the absence of noise, each single type-II ML neuron begins to fire with a nonzero frequency that is relatively insensitive to the change in I_{DC} [46,47]. Here, we consider the subthreshold case of $I_{DC} = 87$ μA/cm^2 where single neurons cannot fire spontaneously without noise.

The last term in Eq. (1a) represents the synaptic coupling of the network. $I_{syn,i}$ of Eq. (2c) represents a synaptic current injected into the ith neuron. The synaptic connectivity is given by the connection weight matrix W ($=\{w_{ij}\}$) where $w_{ij} = 1$ if the neuron j is presynaptic to the neuron i; otherwise, $w_{ij} = 0$. Then, the in-degree of the ith neuron, d_i^{in} (*i.e.*, the number of synaptic inputs to the neuron i) is given by $d_i^{in} = \sum_{j(\neq i)}^{N} w_{ij}$. The coupling strength is controlled by the parameter J, and V_{syn} is the synaptic reversal potential. The synaptic gate variable s obeys the 1st-order kinetics of Eq. (1c) [48,49]. Here the normalized concentration of synaptic transmitters, activating the synapse, is assumed to be an instantaneous sigmoidal function of the membrane potential with a threshold v^* in Eq. (2g), where we set $v^* = 0$ mV and $\delta = 2$ mV. The transmitter release occurs only when the neuron emits a spike (*i.e.*, its potential v is larger than v^*).

Here, we consider the inhibitory synaptic coupling. When the decay time of the synaptic interaction is enough long, mutual inhibition (rather than excitation) may synchronize neural firing activities [50, 51]. By providing a coherent oscillatory output to the principal cells, interneuronal networks play the role of the backbones of many brain oscillations [48,49,52–56]. In this way, interneurons temporally coordinate principal neuron activity and control input and output in principal cells [1]. A majority of locally-connected interneurons coordinate multiple operations in principal cells, while a smaller fraction of long-range interneurons innervate and coordinate all interneuron classes for generation of global synchrony in interneuronal networks [12]. For the inhibitory GABAergic synapse (involving the $GABA_A$ receptors), the synaptic reversal potential is given by $V_{syn} = -80$ mV, the synaptic channel opening rate, corresponding to the inverse of the synaptic rise time τ_r, is $\alpha = 10$ ms^{-1}, and the synaptic closing rate β, which is the inverse of the synaptic decay time τ_d, is $\beta = 0.1$ ms^{-1} [57]. Hence, I_{syn} rises fast and decays slowly.

Numerical integration of Eq. (1) is done using the Heun method [58] (with the time step $\Delta t = 0.01$ ms), and data for (v_i, w_i, s_i) $(i = 1, \ldots, N)$ are obtained with the sampling time interval $\Delta t = 1$ ms. For each realization of the stochastic process in Eq. (1), we choose a random initial point $[v_i(0), w_i(0), s_i(0)]$ for the ith $(i = 1, \ldots, N)$ neuron with uniform probability in the range of $v_i(0) \in (-70, 50)$, $w_i(0) \in (0.0, 0.6)$, and $s_i(0) \in (0.0, 1.0)$.

III. EMERGENCE OF SPARSELY SYNCHRONIZED RHYTHMS ON AN ECONOMICAL SMALL-WORLD NETWORK

In our previous works [11] for both cases of global and random couplings, emergence of sparse synchronization has been investigated by varying the noise intensity D in

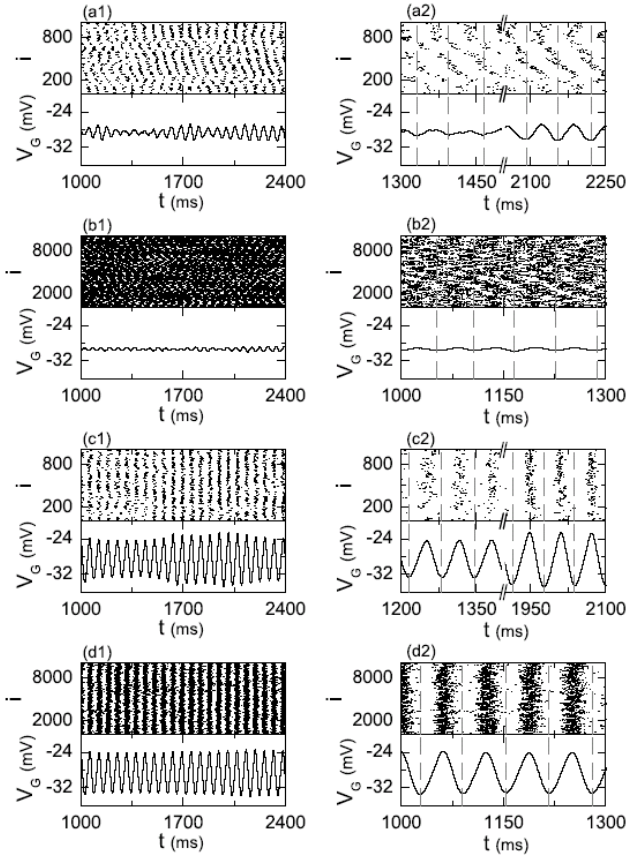

Fig. 1. Unsynchronized population state for $p = 0$: Plots of raster plot of spikes and the global potential V_G versus time t for $N = 10^3$ in (a1) and (a2) [magnification of (a1)] and for $N = 10^4$ in (b1) and (b2) [magnification of (b1)]. Synchronized population state for $p = 0.2$: Plots of raster plot of spikes and the global potential V_G versus time t for $N = 10^3$ in (c1) and (c2) [magnification of (c1)] and for $N = 10^4$ in (d1) and (d2) [magnification of (d1)] in small-world networks of N inhibitory subthreshold ML neurons for $k = 50$, $I_{DC} = 87$, $D = 20$, and $J = 3$. Vertical dashed lines in (a2), (b2), (c2), and (d2) represent the times at which local minima of V_G occur.

neural networks of inhibitory subthreshold ML neurons interacting via real synapses modeled in terms of synaptic kinetics, and sparsely synchronized rhythms have thus been found to appear in a finite range of noise intensity. However, synaptic connections in real neural circuits are known to be sparse, and the connectivity has complex topology which is neither regular nor completely random [12–16]. Hence, we are concerned about the effect of network structure on sparse synchronization in small-world networks which interpolate between the regular lattice and the random graph.

We start with a directed regular ring lattice with N conductance-based ML neurons where each ML neuron is coupled to its first k neighbors ($k/2$ on either side) via outward synapses, and rewire each outward connection at random with probability p such that self-connections and duplicate connections are excluded. Synaptic dynamics between ML neurons are described in terms of kinetics of synaptic gate variables controlled by GABAergic synaptic time constants. Here, we consider a sparse but connected network with a fixed value of $k = 50$. Then, we can tune the network between regularity ($p = 0$) and randomness ($p = 1$). In this way, we investigate emergence of sparsely synchronized rhythm in the directed Watts-Strogatz small-world network of N inhibitory subthreshold ML neurons by varying the rewiring probability p for $I_{DC} = 87$ μA/cm^2, $D = 20$ $\mu\text{A} \cdot \text{ms}^{1/2}/\text{cm}^2$, and $J = 3$ mS/cm^2. (Hereafter, for convenience we omit the dimensions of I_{DC}, D, and J.)

The topological properties of the network architecture has already been well characterized in terms of the clustering coefficient $C(p)$ (local property) and the average path length $L(p)$ (global property) [37]. Here, the clustering coefficient which represents the cliquishness of a typical neighborhood in the network characterizes the local efficiency of information transfer, while the average path length $L(p)$ which denotes the typical separation between two vertices in the network characterize the global efficiency of information transfer. The regular lattice ($p = 0$) is highly clustered but large world where L grows linearly with N, while the random graph ($p = 1$) is poorly clustered but small world where L grows logarithmically with N [37]. As soon as p increases from zero, $L(p)$ decreases dramatically, which results in the emergence of a small-world phenomenon (as in the random graph) which is popularized by the phrase of the six degrees of separation [59,60]. However, during this dramatic drop in $L(p)$, $C(p)$ remains almost constant at its value for the regular lattice. Consequently, for small p small-world networks with high clustering and short path lengths appear [37].

By increasing p, we now investigate the effect of the network architecture on emergence of sparsely synchronized rhythm. Collective spike synchronization may be well visualized in the raster plot of neural spikes and well described by using the (population-averaged) global potential

$$V_G(t) = \frac{1}{N} \sum_{i=1}^{N} v_i(t). \tag{3}$$

In the thermodynamic limit ($N \to \infty$), a population state becomes synchronized if an oscillating global potential V_G appears. Otherwise (*i.e.*, when V_G is stationary), it becomes unsynchronized. Figure 1 shows the raster plots of spikes and the global potential V_G for $p = 0$ and 0.2. By increasing N, we first investigate the population state in the regular lattice for $p = 0$. As shown in Fig. 1(a1) for $N = 10^3$, the raster plot shows a zigzag pattern intermingled with inclined partial stripes of spikes with diverse inclinations and widths, and V_G is composed of coherent parts with regular large-amplitude oscillations and incoherent parts with irregular small-amplitude fluctuations; coherent and incoher-

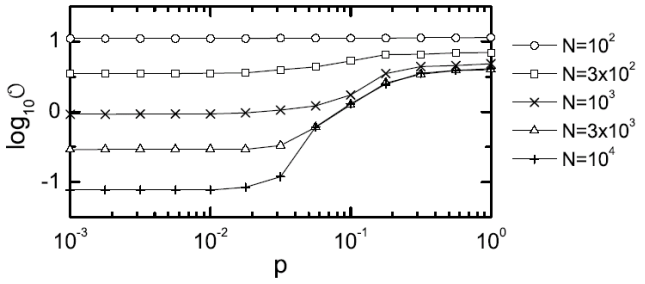

Fig. 2. Synchronous Transition. Plot of $\log_{10}\mathcal{O}$ versus p in small-world networks of N inhibitory subthreshold ML neurons for $k = 50$, $I_{DC} = 87$, $D = 20$, and $J = 3$.

ent parts are clearly shown in the magnified Fig. 1(a2). For $p = 0$, the clustering coefficient is high, and hence partial stripes (indicating local clustering of spikes) seem to appear in the raster plot of spikes. As N is increased to 10^4, the amplitude of V_G becomes smaller, and the duration of incoherent parts becomes longer [see Fig. 1(b1)]. In the magnified Fig. 1(b2), partial stripes become more inclined from the vertical, and hence spikes become more difficult to keep pace with each other. As a result, V_G shows a noisy fluctuations with smaller amplitudes. Hence the population state for $p = 0$ seems to be unsynchronized because V_G tends to be nearly stationary as N increases to the infinity. As p is increased, long-range short-cuts begin to appear, and hence characteristic path length becomes shorter. Consequently, for sufficiently large p we expect emergence of synchronized population state because global efficiency of information transfer becomes better. As an example, we consider the case of $p = 0.2$. For $N = 10^3$, V_G shows a regular oscillation, as shown in Fig. 1(c1) and 1(c2). Its amplitudes are much larger than that for the case of $p = 0$, although there is a little variation in the amplitude. To understand the behavior of V_G better, we look into the magnified raster plot of spikes in Fig. 1(c2). We note that the raster plot of spikes is composed of nearly vertically-aligned partial stripes in each oscillating cycle (*i.e.*, the degree of zigzagness for partial stripes is much reduced), in contrast to the $p = 0$ case. A little zigzagness is shown in the partial stripes near $t = 1300$ ms, unlike the case near $t = 2000$ ms, and hence the amplitude of V_G near $t = 2000$ ms becomes larger than that near $t = 1300$ ms. We next examine the behavior of V_G for $N = 10^4$. As shown in Fig. 1(d1), V_G shows regular oscillations, and the amplitudes in each oscillating cycle are nearly the same, in contrast to the case of $N = 10^3$. In each oscillating cycle, partial stripes are nearly vertically aligned, and hence the zigzagness degree is nearly the same. Hence, V_G displays more regular oscillations with nearly the same amplitudes. Consequently, the population state for $p = 0.2$ seems to be synchronized because V_G tend to show regular oscillations as N goes to the infinity.

As is well known, the mean square deviation of the

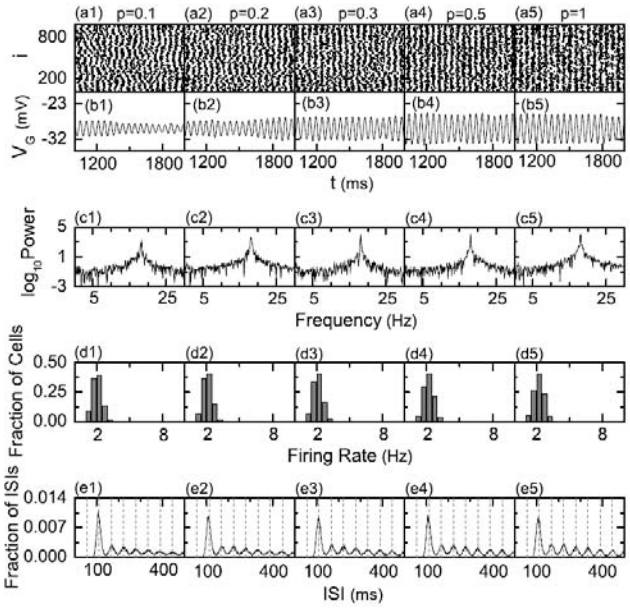

Fig. 3. Sparsely synchronized states for various values of p. Raster plots of neural spikes versus t in (a1)-(a5), plots of V_G versus t in (b1)-(b5), power spectra in (c1)-(c5) (each power spectrum of V_G is calculated with 2^{13} data), distribution of single cell firing rates across the population in (d1)-(d5) (firing rates of individual neurons are calculated through 10^4 ms time-averaging and the bin size for the histogram is 0.5 Hz), and interspike intervals (ISIs) histogram in (e1)-(e5) (each ISI histogram is composed of 5×10^4 ISIs and the bin size for the histogram is 5 ms) in small-world networks of N ($= 10^3$) inhibitory subthreshold ML neurons for $k = 50$, $I_{DC} = 87$, $D = 20$, and $J = 3$. Vertical dashed lines in (e1)-(e5) denote integer multiples of the global period T_G ($\simeq 56$ ms).

global potential V_G (*i.e.*, time-averaged fluctuations of V_G),

$$\mathcal{O} \equiv \overline{(V_G(t) - \overline{V_G(t)})^2}, \tag{4}$$

where the overbar represents the time average, plays the role of an order parameter used for describing the synchrony-asynchrony transition [61]. For the synchronized (unsynchronized) state, the order parameter $\mathcal{O}$ approaches a non-zero (zero) limit value as N goes to the infinity. Figure 2 shows a plot of the order parameter versus the rewiring parameter p. For $p < p_{th}$ ($\simeq 0.044$), unsynchronized states exist because the order parameter $\mathcal{O}$ tends to zero as $N \to \infty$. As p passes the threshold p_{th}, a synchronous transition occurs because the values of $\mathcal{O}$ become saturated to non-zero limit values for $N \geq 3 \cdot 10^3$. These synchronized states seem to appear because global efficiency of information transfer between distant neurons for $p > p_{th}$ become enough for emergence of population synchronization.

We now examine the population and individual behaviors of synchronized states for various values of $p > p_{th}$. By varying p, we characterize both the population behaviors in terms of their global potential V_G and their

power spectra and the individual behaviors in terms of the firing-rate distribution of individual neurons. By comparing the population and individual behaviors, one can understand sparsely synchronized states well. As shown in Figs. 3(a1)-(a5) and Figs. 3(b1)-(b5), the zigzagness degree of partial stripes in the raster plots of spikes becomes reduced as p is increased, and eventually for $p = p_{max}$ (~ 0.5), the raster plot becomes composed of vertical stripes without zigzag, and then the pacing degree between spikes becomes nearly the same. Hence, the amplitude of V_G increases up to p_{max}, and then its value becomes saturated. Figures 3(c1)-(c5) show power spectra of V_G with peaks at population frequencies f_p ($\simeq 18$) Hz. Hence, the population oscillations correspond to beta rhythms. In contrast to population rhythm, individual neurons discharge intermittent and stochastic spikings as Geiger counters. As shown in Figs. 3(d1)-(d5) the average spiking frequency of individual neurons is about 2 Hz, and hence each neuron makes an average firing very sparsely once during 9 population cycles. To further investigate the individual behaviors, we collect 5×10^4 interspike intervals (ISIs) from all individual neurons and get the ISI histograms which are shown in Figs. 3(e1)-(e5). Multiple peaks appear at multiples of the period T_G ($= 1/f_G \simeq 56$ ms) of the global potential V_G. However, due to appearance of preparatory cycles, the 1st peak of the histogram (which is the highest one) appears at 2 T_G (not T_G) [11]. Hence, individual neurons fire mostly in alternate global cycles. In this way, individual neurons exhibit stochastic phase locking leading to stochastic spike skipping (*i.e.*, intermittent spikings phase-locked to V_G at random multiples of the period of V_G). Consequently, for $p > p_{th}$ sparsely synchronized rhythms emerge.

With increasing p above p_{th}, synchrony degree is increased because global efficiency of information transfer becomes better. However, as p is increased, the network axon wiring length becomes longer due to long-range short-cuts. Longer axonal connections are expensive because of material and energy costs. Hence, in view of dynamical efficiency we search for optimal population rhythm emerging at a minimal wiring cost. An optimal rhythm may emerge through tradeoff between the synchrony degree and the wiring cost. We first measure the synchrony degree by using a statistical-mechanical spike-based synchronization measure introduced in our previous works [11]. As shown in Figs. 3(a1)-(a5), population synchronization may be well visualized in a raster plot of spikes. For a synchronized case, the raster plot is composed of partially-occupied stripes (indicating sparse synchronization). To measure the degree of the population synchronization seen in the raster plot, a spike-based measure M was introduced by considering the occupation pattern and the pacing pattern of the spikes in the stripes [11]. The spiking coherence measure M_i of the ith stripe is defined by the product of the occupation degree O_i of spikes (representing the density of the ith stripe) and the pacing degree P_i of spikes (denoting the smearing of the ith stripe):

$$M_i = O_i \cdot P_i. \tag{5}$$

The occupation degree O_i in the ith stripe is given by the fraction of spiking neurons:

$$O_i = \frac{N_i^{(s)}}{N}, \tag{6}$$

where $N_i^{(s)}$ is the number of spiking neurons in the ith stripe. For sparse synchronization, $O_i < 1$, while for full synchronization, $O_i = 1$. The pacing degree P_i of each microscopic spike in the ith stripe can be determined in a statistical-mechanical way by taking into consideration its contribution to the macroscopic global potential V_G. Each global cycle of V_G begins from its left minimum, passes the central maximum, and ends at the right minimum; the central maxima coincide with centers of stripes in the raster plot [see Figs. 3(a1)-(a5)]. An instantaneous global phase $\Phi(t)$ of V_G is introduced via linear interpolation in the two successive subregions forming a global cycle. The global phase $\Phi(t)$ between the left minimum (corresponding to the beginning point of the ith global cycle) and the central maximum is given by

$$\Phi(t) = 2\pi(i - 3/2) + \pi \left(\frac{t - t_i^{(min)}}{t_i^{(max)} - t_i^{(min)}} \right) \quad \text{for} \quad t_i^{(min)} \le t < t_i^{(max)} \quad (i = 1, 2, 3, \dots), \tag{7}$$

and $\Phi(t)$ between the central maximum and the right minimum (corresponding to the beginning point of the $(i+1)$th cycle) is given by

$$\Phi(t) = 2\pi(i - 1) + \pi \left(\frac{t - t_i^{(max)}}{t_{i+1}^{(min)} - t_i^{(max)}} \right) \quad \text{for} \quad t_i^{(max)} \le t < t_{i+1}^{(min)} \quad (i = 1, 2, 3, \dots), \tag{8}$$

where $t_i^{(min)}$ is the beginning time of the ith global cycle (*i.e.*, the time at which the left minimum of V_G appears in the ith global cycle) and $t_i^{(max)}$ is the time at which the maximum of V_G appears in the ith global cycle. Then, the contribution of the kth microscopic spike in the ith stripe occurring at the time $t_k^{(s)}$ to V_G is given by $\cos \Phi_k$, where Φ_k is the global phase at the kth spiking time [*i.e.*, $\Phi_k \equiv \Phi(t_k^{(s)})$]. A microscopic spike makes the most constructive (in-phase) contribution to V_G when the corresponding global phase Φ_k is $2\pi n$ ($n = 0, 1, 2, \dots$) while it makes the most destructive (anti-phase) contribution to V_G when Φ_i is $2\pi(n - 1/2)$. By averaging the contributions of all microscopic spikes in the ith stripe to V_G, we obtain the pacing degree of spikes in the ith stripe:

$$P_i = \frac{1}{S_i} \sum_{k=1}^{S_i} \cos \Phi_k, \tag{9}$$

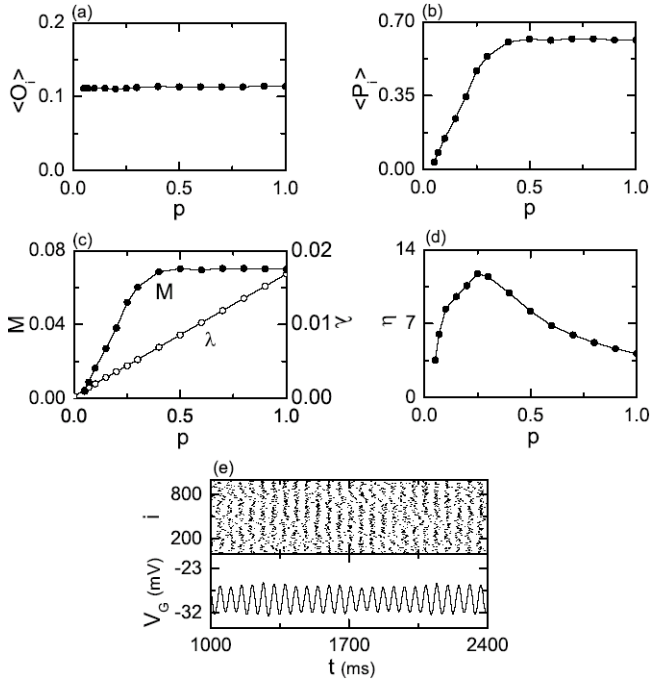

Fig. 4. Emergence of optimally sparsely synchronized rhythm in an economic small-world network. (a) Plot of the average occupation degree $\langle O_i \rangle$ versus p. (b) Plot of the average pacing degree $\langle P_i \rangle$ versus p. (c) Plot of the synchrony measure M and normalized wiring length λ versus p. (d) Dynamical efficiency η versus p. (e) Raster plot of neural spikes and plot of V_G versus t at an optimal value p^*_{DE} ($\simeq 0.24$) in small-world networks of N ($= 10^3$) inhibitory subthreshold ML neurons for $k = 50$, $I_{DC} = 87$, $D = 20$, and $J = 3$.

where S_i is the total number of microscopic spikes in the ith stripe. By averaging M_i of Eq. (5) over a sufficiently large number N_s of stripes, we obtain the spike-based coherence measure M:

$$M = \frac{1}{N_s} \sum_{i=1}^{N_s} M_i. \tag{10}$$

By varying p, we follow 3×10^3 stripes and characterize sparse synchronization in terms of $\langle O_i \rangle$ (average occupation degree), $\langle P_i \rangle$ (average pacing degree), and the spiking measure M for 14 values of p in the sparsely synchronized region, and the results are shown in Figs. 4(a)-(c). We note that the average occupation degree $\langle O_i \rangle$ (denoting the average density of stripes in the raster plot) is nearly the same ($\langle O_i \rangle \simeq 0.11$), independently of p; only a fraction (about 1/9) of the total neurons fire in each stripe [see Figs. 3(a1)-(a5)]. This partial occupation in the stripes results from stochastic spike skipping of individual neurons and is seen well in the multi-peaked ISI histograms [see Figs. 3(e1)-(e5)]. The average occupation degree ($\langle O_i \rangle \simeq 0.11$) implies that individual neurons fire about once during the nine global cycles, which agrees well with the average firing rates ($\simeq 2$ Hz) of individual neurons shown in Figs. 3(d1)-(d5). Hence, the average occupation degree $\langle O_i \rangle$ characterize the sparseness degree of population synchronization well. On the other hand, with increasing p, the average pacing degree $\langle P_i \rangle$ increases rapidly due to appearance of long-range connections. However, the value of $\langle P_i \rangle$ saturates for $p = p_{max}$ (~ 0.5) because long-range shortcuts which appear up to p_{max} play sufficient role to get maximal pacing degree. Figure 4(c) shows the spiking measure M (taking into consideration both the occupation pattern and the pacing pattern of spikes) versus p. As in the case of $\langle P_i \rangle$, M makes a rapid increase up to $p = p_{max}$, because $\langle O_i \rangle$ is nearly independent of p. $M(p)$ is nearly equal to $\langle P_i \rangle /9$ because of the sparse occupation [$\langle O_i \rangle \simeq 0.11$]. We next calculate the wiring length by varying p on a ring of radius R ($=N/2\pi$) where neurons are placed equidistantly. The axonal wiring length, Λ_{ij}, between neuron i and neuron j is given by the arc length between two vertices i and j on the ring:

$$\Lambda_{ij} = \begin{cases} |j-i| \text{ for } |j-i| \le \frac{N}{2} \\ N - |j-i| \text{ for } |j-i| > \frac{N}{2}. \end{cases} \tag{11}$$

Then, the total wiring length is:

$$\Lambda_{total} = \sum_{i=1}^{N} \sum_{j=1(j\neq i)}^{N} a_{ij} \cdot \Lambda_{ij}, \tag{12}$$

where a_{ij} is the ij element of the adjacency matrix A of the network. The connection between vertices in the network is represented by its $N \times N$ adjacency matrix A ($= \{a_{ij}\}$) whose element values are 0 or 1. If $a_{ij} = 1$, then an edge from the vertex i to the vertex j exists; otherwise no such edges exists. This adjacency matrix A corresponds to the transpose of the connection weight matrix W in Sec. II. We get a normalized wiring length λ by dividing Λ_{total} with $\Lambda^{(global)}_{total}$ [$= \sum_{i=1}^{N} \sum_{j=1(j\neq i)}^{N} \Lambda_{ij}$] which is the total wiring length for the global-coupled case:

$$\lambda = \frac{\Lambda_{total}}{\Lambda^{(global)}_{total}}. \tag{13}$$

Plot of λ versus p is shown in Fig. 4(c). It increases linearly with respect to p. Hence, with increasing p, the wiring cost becomes expensive, while the synchrony degree increases. An optimal rhythm may emerge via tradeoff between the synchrony degree M and the wiring cost. To this end, a dynamical efficiency η is introduced in [12]:

$$\eta = \frac{\text{Synchrony Degree } (M)}{\text{Normalized Wiring Length } (\lambda)}. \tag{14}$$

Figure 4(d) shows plot of η versus p. For $p = p^*_{DE}$ ($\simeq 0.24$), an optimal rhythm is found to emerge at a minimal wiring cost in an economic small-world network. Optimally sparsely synchronized rhythm is shown in Fig. 4(e). Since the economical small-world network

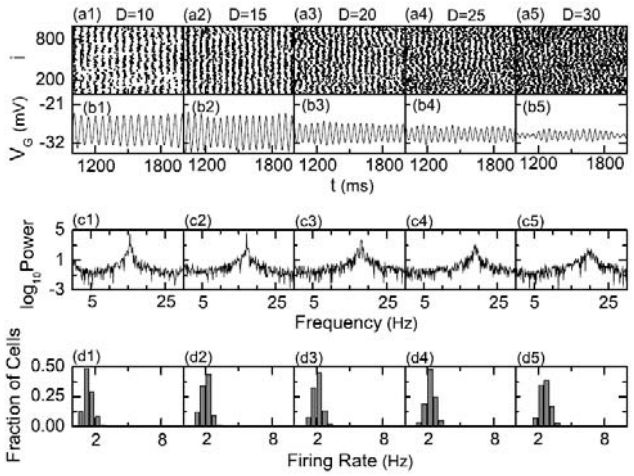

Fig. 5. Sparsely synchronized states for various values of D when $p = 0.24$. Raster plots of neural spikes versus t in (a1)-(a5), plots of V_G versus t in (b1)-(b5), power spectra in (c1)-(c5) (each power spectrum of V_G is calculated with 2^{13} data), and distribution of single cell firing rates across the population in (d1)-(d5) (firing rates of individual neurons are calculated through 10^4 ms time-averaging and the bin size for the histogram is 0.5 Hz) in small-world networks of N ($= 10^3$) inhibitory subthreshold ML neurons for $k = 50$, $I_{DC} = 87$, $J = 3$, and $p = 0.24$.

has a moderate clustering coefficient $C(p^*_{DE})$ ($= 0.31$), the raster plot of spikes shows a zigzag pattern due to local clustering of spikes, and V_G exhibits a regular oscillation at a population frequency f_G ($= 18$ Hz).

So far, we consider the case of noise intensity of $D = 20$. To examine the robustness of the sparsely synchronized rhythm for $D = 20$, we fix the value of the rewiring probability p at $p = p^*_{DE}$ ($= 0.24$), and study emergence of sparsely synchronized rhythm by varying D. Through calculation of the order parameter $\mathcal{O}$ of Eq. 4, sparsely synchronized is found to exist in a finite range of intermediate noise intensity ($8.5 < D < 37$), as in our previous works [11] for both cases of global and random couplings. When passing the lower threshold value ($D \simeq 8.5$) population synchronization occurs due to a constructive role of noise, while such population synchronization breaks up due to a destructive role of noise when passing the higher threshold value ($D \simeq 37$). Figures 5 (a1)-(a2) and Figs. 5(b1)-(b2) show the raster plots of spikes and the global potentials V_G for various values of D in the synchronized region. Stripes in the raster plots and oscillating V_G show sparsely synchronized states. The population frequencies of the synchronized rhythms for $D = 10, 15, 20, 25$, and 30 are 16, 17, 18, 19, and 19Hz, respectively, as shown in Figs. 5(c1)-(c5). On the other hand, average firing rates of individual neurons for $D = 10, 15, 20, 25$, and 30 are 1.4, 2, 2, 2.3, and 2.6Hz, respectively, as shown in Figs. 5(d1)-(d5), which are much less than the population frequencies. Consequently, sparsely synchronized rhythms appear in a finite range of noise intensity D, as in both cases of global and random couplings [11].

IV. SUMMARY

We have investigated the effect of network architecture on emergence of sparsely synchronized rhythm by increasing the rewiring probability p in a small-world network of inhibitory subthreshold conductance-based ML neurons interacting via real synapses modeled in terms of kinetics coordinated by the GABAergic synaptic time constants. For $p = 0$, global efficiency of information transfer is low because of long synaptic path length, and hence an unsynchronized state appears. As p is increased, long-range connections begin to appear, and then average path length becomes shorter. When passing a critical value p_{th} ($= 0.044$), the unsynchronized state becomes destabilized and a sparsely synchronized rhythm emerges. This dynamical critical value, p_{th}, is determined through calculation of the dynamical order parameter. For a synchronized case, the raster plot of neural spikes shows a zigzag pattern intermingled with inclined partial stripes which seem to appear due to high local clustering, and an ensemble-averaged small-amplitude potential V_G is found to oscillate with population frequency of 18 Hz. However, individual neurons discharge spikes irregularly at low rates (~ 2 Hz) which is much lower than the population frequency. With increasing p, the zigzag degree of partial stripes decreases in the raster plot (*i.e.*, the inclination of partial stripes from the vertical line becomes smaller), and hence the synchrony degree between spikes (*i.e.*, amplitude of V_G) increases. For $p = p_{max}$ (~ 0.5), the raster plot becomes composed of vertical stripes without zigzag, and then the synchrony degree reaches a saturated peak value. This kind of sparse synchronization is well characterized in terms of the average occupation degree, the pacing degree, and the synchrony degree introduced in our previous works [11]. On the other hand, as p is increased network axon wiring length becomes longer because more long-range connections appear. Hence, wiring economy must be taken into consideration for dynamical efficiency. A ratio of the synchrony degree to the geometrical wiring cost is found to be maximal at a dynamical-efficiency critical value p^*_{DE} ($\simeq 0.24$) (less than p_{max}). For this case, an optimally sparsely synchronized rhythm is found to emerge at a minimal wiring cost in an economic small-world network. Finally, we also examined the noise effect on sparse synchronization for $p = p^*_{DE}$. Thus, partially synchronized rhythms are found to appear in a finite range of intermediate noise intensity, as in both cases of global and random couplings [11].

REFERENCES

[1] G. Buzsáki, *Rhythms of the Brain* (Oxford University Press, New York, 2006).
[2] R. D. Traub and M. A. Whittington, *Cortical Oscillations in Health and Diseases* (Oxford University Press, New York, 2010).
[3] X.-J. Wang, Physiol. Rev. **90**, 1195 (2010).
[4] A. Fisahn, F. G. Pike, E. H. Buhl and O. Paulsen, Nature **394**, 186 (1998).
[5] J. Csicsvari, H. Hirase, A. Czurko and G. Buzsáki, Neuron **21**, 179 (1998).
[6] P. Fries, J. H. Reynolds, A. E. Rorie and R. Desimone, Science **291**, 1560 (2001).
[7] M. Steriade, D. McCormick and T. Sejnowski, Science **262**, 679 (1993).
[8] A. Destexhe and T. J. Sejnowski, Physiol. Rev. **83**, 1401 (2003).
[9] X.-J. Wang, in *Encyclopedia of Cognitive Science*, edited by L. Nadel (MacMillan, London, 2003), p. 272.
[10] N. Brunel and V. Hakim, Chaos **18**, 015113 (2008); N. Brunel and V. Hakim, Neural Comput. **11**, 1621 (1999); N. Brunel, J. Comput. Neurosci. **8**, 183 (2000); N. Brunel and X.-J. Wang, J. Neurophysiol. **90**, 415 (2003); C. Geisler, N. Brunel and X.-J. Wang, J. Neurophysiol. **94**, 4344 (2005); N. Brunel and D. Hansel, Neural Comput. **18**, 1066 (2006).
[11] W. Lim and S.-Y. Kim, J. Comput. Neurosci. **31**, 667 (2011); D.-G. Hong, S.-Y. Kim and W. Lim, J. Korean Phys. Soc. **59**, 2840 (2011); S.-Y. Kim, D.-G. Hong, J. Kim and W. Lim, J. Phys. A **45**, 155102 (2012).
[12] G. Buzsáki, C. Geisler, D. A. Henze and X.-J. Wang, Trends in Neurosciences **27**, 186 (2004).
[13] D. B. Chklovskii, B. W. Mel and K. Svoboda, Nature **431**, 782 (2004).
[14] S. Song, P. J. Sjöström, M. Reigl, S. Nelson and D. B. Chklovskii, PLoS Biol. **3**, E68 (2005).
[15] P. Larimer and B. W. Strowbridge, J. Neurosci. **28**, 12212 (2008).
[16] E. Bullmore and O. Sporns, Nat. Rev. Neurosci. **10**, 186 (2009).
[17] R. Albert and A. L. Barabasi, Rev. Mod. Phys. **74**, 47 (2002).
[18] X. F. Wang and G. Chen, IEEE Cir. Sys. Mag. **3**, 6 (2003).
[19] O. Sporns, G. Tononi and G. M. Edelman, Cereb. Cortex **10**, 127 (2000).
[20] L. F Lago-Fernández, R. Huerta, F. Corbacho and J. A. Sigüenza, Phys. Rev. Lett. **84**, 2758 (2000).
[21] O. Kwon, H. T. Moon, Phys. Lett. A **298**, 319 (2002).
[22] A. Roxin, H. Riecke and S. A. Solla, Phys. Rev. Lett. **92**, 198101 (2004).
[23] M. Kaiser and C. C. Hilgetag, PLoS Comp. Biol. **2**, e95 (2006).
[24] H. Riecke, A. Roxin, S. Madruga and S. Solla, Chaos **17**, 026110 (2007).
[25] S. Achard and E. T. Bullmore, PLoS Comp. Biol. **3**, e17 (2007).
[26] S. Yu, D. Huang, W. Singer and D. Nikolie, Cereb. Cortex **18**, 2891 (2008).
[27] Q. Wang, Z. Duan, M. Perc and G. Chen, EPL **83**, 50008 (2008).
[28] M. Shanahan, Phys. Rev. E **78**, 041924 (2008).
[29] M. Ozer, M. Perc and M. Uzuntarla, Phys. Lett. A **373**, 964 (2009).
[30] Q. Wang, M. Perc, Z. Duan and G. Chen, Physica A **389**, 3290 (2010).
[31] J. T. Lizier, S. Pritam and M. Prokopenko, Artificial Life **17**, 293 (2011).
[32] C. A. S. Batista, A. M. Batista, J. A. C. de Pontes, R. L. Viana and S. R. Lopes, Phys. Rev. E **76**, 016218 (2007).
[33] R. J. Morgan and I. Soltesz, Proc. Natl. Acad. Sci. USA **105**, 6179 (2008).
[34] P. Bonifazi, M. Goldin, M. A. Picardo, I. Jorquera, A. Cattani, G. Bianconi, A. Represa, Y. Ben-Ari and R. Cossart, Science **326**, 1419 (2009).
[35] Q. Wang, M. Perc. Z. Duan and G. Chen, Phys. Rev. E **80**, 026206 (2009).
[36] Q. Wang, G. Chen and M. Perc, PLoS ONE **6**, e15851 (2011).
[37] D. J. Watts and S. H. Strogatz, Nature **393**, 440 (1998).
[38] V. Latora and M. Marchiori, Phys. Rev. Lett. **87**, 198701 (2001); Eur. Phys. J. B **32**, 249 (2003).
[39] S. B. Laughlin and T. J. Sejnowski, Science **301**, 1870 (2003).
[40] D. B. Chklovskii, T. Schikorski and C. F. Stevens, Neuron **34**, 341 (2002).
[41] D. B. Chklovskii and A. A. Koulakov, Annu. Rev. Neurosci. **27**, 369 (2004).
[42] D. B. Chklovskii, Neuron **43**, 609 (2004).
[43] S. Achard and E. Bullmore, PLoS Comp. Biol. **3**, e17 (2007).
[44] E. Bullmore and O. Sporns, Nat. Rev. Neurosci. **13**, 336 (2012).
[45] C. Morris and H. Lecar, Biophys. J. **35**, 193 (1981).
[46] J. Rinzel and B. Ermentrout, in *Methods in Neural Modeling: from Ions to Networks*, edited by C. Koch and I. Segev (MIT Press, Cambridge, 1998), p. 251.
[47] A. L. Hodgkin, J. Physiol. **107**, 165 (1948).
[48] D. Golomb and J. Rinzel, Physica D **72**, 259 (1994).
[49] X.-J. Wang and G. Buzsáki, J. Neurosci. **16**, 6402 (1996).
[50] C. van Vreewijk, L. F. Abbott and G. B. Ermentrout, J. Comput. Neurosci. **1**, 313 (1994).
[51] D. Hansel, G. Mato and C. Meunier, Neural Comput. **7**, 307 (1995).
[52] X.-J. Wang and J. Rinzel, Neural Comput. **4**, 84 (1992).
[53] J. White, C. C. Chow, J. Ritt, C. Soto-Trevino and N. Kopell, J. Comput. Neurosci. **5**, 5 (1998).
[54] M. A. Whittington, R. D. Traub, N. Kopell, B. Ermentrout and E. H. Buhl, Int. J. Psychophysiol. **38**, 315 (2000).
[55] P. H. E. Tiesinga, J.-M. Fellous, J. V. Jose and T. J. Sejnowski, Hippocampus **11**, 251 (2001).
[56] G. Buzsáki and X.-J. Wang, Annu. Rev. Neurosci. **35**, 203 (2012).
[57] C. Börgers and N. Kopell, Neural Comput. **15**, 509 (2003); *ibid.* **17**, 557 (2005).
[58] M. San Miguel and R. Toral, in *Instabilities and Nonequilibrium Structures VI*, edited by J. Martinez, R. Tiemann, and E. Tirapegui (Kluwer Academic Publisher, Dordrecht, 2000), p. 35.
[59] S. Milgram, Psychology Today **1**, 61 (1967).
[60] J. Guare, *Six Degrees of Separation: A Play* (Random House, New York, 1990).
[61] S. C. Manrubia, A. S. Mikhailov and D. H. Zanette,

Emergence of Dynamical Order (World Scientific, Singapore, 2004).
[62] W. Lim and S.-Y. Kim, J. Korean Phy. Soc. **57**, 1290 (2010).